Applied Surface Science 639 (2023) 158231

Contents lists available at ScienceDirect

Applied Surface Science

journal homepage: www.elsevier.com/locate/apsusc

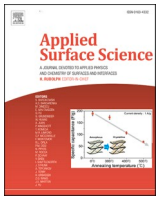

Full Length Article

Electron-stimulated desorption kinetics of ultra-thin LiCl films on graphene

Jon Azpeitia [a,*], Michael Foerster [b], Lucía Aballe [b], Mar García-Hernández [a], José Ángel Martín-Gago [a], Pablo Merino [a], Irene Palacio [a,*]

[a] Instituto de Ciencia de Materiales de Madrid (ICMM-CSIC), Sor Juana Inés de la Cruz 3, Cantoblanco, 28049 Madrid, Spain
[b] ALBA Synchrotron, Carrer de la llum 2-26, Cerdanyola del Vallés, 08290 Barcelona, Spain

A B S T R A C T

Ultra-thin alkali halide films are an important substrate for studying single quantum objects at the atomic scale, as they serve as decoupling scaffolds. However, their stability upon exposure to electrons and photons, the most common probes used to study nanomaterials, is not fully understood. Here we present a study of the evolution of the structure of ultra-thin LiCl films, grown on graphene, upon low-energy electron irradiation by means of microspot-low-energy electron diffraction and microscopy. We find that the intensity of the LiCl diffraction spots irradiated at various electron energies follows a bi-exponential decay function, which can be rationalized by two different desorption regimes. In addition, we detect a change in the work function caused by the electron irradiation, confirming desorption of the LiCl film from the graphene layer. We understand the underlying mechanisms for the electron-induced desorption of the salt film in terms of the evolution of the elementary quasiparticles involved in the process: holes, excitons and F and H center pairs. Moreover, a direct comparison of the electron-induced and the soft X-ray photon-induced processes reveal that, in addition to LiCl desorption, the intercalation of lithium into graphene reported for X-ray induced desorption does not take place in electron-stimulated desorption.

1. Introduction

Insulating thin films on metals have attracted great interest due to their applicability in the study of 2D materials and 2D heterostructures [1]. They are optimal layers to electronically isolate nanomaterials from metallic substrates, allowing the study and manipulation of single atoms [2], molecules [3], nanoparticles [4] and nanostructures. Among them, alkali halide thin films, such as NaCl and LiCl have demonstrated a broad utility for many 2D applications: they can act as protective layers for graphene [5], as ultrathin insulating layers [6] or as precursors for sodium and lithium intercalation under epitaxial 2D materials [7,8].

Thin alkali halide films can be epitaxially grown on metallic and insulating substrates by physical vapor deposition (PVD), preserving their stoichiometry. They weakly interact with most substrates, which permits to characterize their intrinsic properties. When alkali halides are irradiated with either photons [9] or electrons [10–13], primary excitations, i. e. unbounded and bounded electron-hole pairs (excitons) are efficiently formed. These hot quasiparticles relax by interacting with phonons and form Frenkel defects, i. e. F- and H- center pairs [14], which results in efficient desorption of both alkali and halogen atoms. However, differences in the desorption processes when photons and electrons are used are not yet well understood and several microscopic models have been proposed to describe the electron-/photon-induced desorption of alkali halides on various substrates [15–20]. In addition, electrons are, together with photons, among the most employed probes in the analysis of materials, the study of ultra-thin LiCl grown on graphene upon low- energy electron irradiation provide crucial information extendable to other 2D heterostructures that involve not only alkali halide thin films on graphene, but on other sort of 2D materials such as hexagonal boron nitride (h-BN) [21] and transition metal dichalcogenides (TMDs) [22].

In this work, we study the desorption mechanisms of ultra-thin LiCl films on graphene grown on Ir(1 1 1) upon low-energy electron irradiation. The intensity evolution of the LiCl low-energy electron diffraction (LEED) pattern during irradiation permits us to characterize the desorption kinetics of the films upon irradiation with electrons of different kinetic energies (ranging from 27 eV to 163 eV). These energies lie above the electron-stimulated desorption (ESD) threshold, fixed by the minimum energy for surface and bulk exciton and hole formation in alkali halides [14,23–25]. We demonstrate that there are two different desorption regimes that lead to a desorption efficiency decline over time. In addition, we compare electron-stimulated desorption with photon-induced desorption to gain further insights into the desorption processes of alkali halide films on surfaces and observe that the latter follows a single time constant kinetics.

* Corresponding authors.
E-mail addresses: jon.azpeitia@icmm.csic.es (J. Azpeitia), i.palacio@csic.es (I. Palacio).

https://doi.org/10.1016/j.apsusc.2023.158231
Received 8 June 2023; Received in revised form 10 August 2023; Accepted 10 August 2023
Available online 15 August 2023

2. Experimental methods

Sample preparation and experiments were performed at the Low-Energy Electron Microscopy/Photoemission Electron Microscopy (LEEM/PEEM) end station of the CIRCE beamline in ALBA Synchrotron [26]. Samples were prepared in ultra-high vacuum (UHV) at a base pressure $\leq 1x10^{-10}$ mbar. Ir(1 1 1) surfaces were cleaned with several cycles of Ar^{+} sputtering and thermal annealing in oxygen atmosphere (T = 1100 °C and P = $2x10^{-8}$ mbar). The last annealing was performed in UHV to prevent residual oxides on the surface. Graphene (Gr) was grown on Ir(1 1 1) using ethylene as carbon precursor. The growth protocol is as follows: Ir(1 1 1) is exposed to ethylene (P = $1x10^{-8}$ mbar) for 30 s at room temperature and afterwards it is flashed up to 1100 °C. The substrate is then again exposed to ethylene (P = $1x10^{-7}$ mbar) and annealed at 1100 °C for 7 min. We monitor the temperature of the substrate with a Tungsten Rhenium (WRe) thermocouple attached to the commercial sample-holder (ELMITEC Elektronenmikroskopie GmbH) in close proximity to the Ir(1 1 1) crystal. Following this recipe a homogeneous monolayer of Gr is observed on the Ir(1 1 1) surface [27], with no rotational mismatch with the Ir(1 1 1) surface structure in comparison with other works [28]. LiCl thin films were grown on Gr/Ir(1 1 1) by sublimating LiCl (≥ 99.98%, Sigma-Aldrich) from a home-made tantalum crucible held at 450 °C, keeping the Gr/Ir(1 1 1) at room temperature. The temperature of the crucible was controlled with a K-type thermocouple directly spot-welded to the crucible. For LEED experiments we employed a 10 μm diameter illumination aperture and for Mirror Electron Mode (MEM) and LEEM experiments we used a Field of View (FoV) of 50 μm.

3. Results and discussion

Fig. 1 a) shows a LEED pattern (electron energy E = 65 eV) of a pristine ultra-thin LiCl film grown on top of Gr/Ir(1 1 1). The pattern is dominated by a ring-shaped intensity maximum (orange arrow) that corresponds to the LiCl lattice parameter (a = 2.56 Å). The observation of a ring rather than a collection of discrete maxima is indicative of multiple rotational domains coexisting on the surface of the inspected zone (10 μm illumination aperture). The Ir(1 1 1) and the graphene spots are not resolved, which can be explained by a LiCl film thickness exceeding the penetration depth of the impinging electrons (i. e. film thicker than ≈ 4 monolayers). We assign this coverage as the initial stage for irradiation experiments. Fig. 1 b) shows a LEED pattern of the same sample after 900 s of electron irradiation. The Ir(1 1 1), graphene (indicated by green and blue arrows, respectively) and the characteristic moiré pattern diffraction spots are now fully resolved while the LiCl-related ring is no longer present, indicating full desorption of the thin film. We assign this LEED configuration as the final stage of irradiation experiments as no further changes are observed, regardless of how much longer the sample is exposed to electrons. Fig. 1 c) presents the intensity evolution of the LiCl ring feature as a function of irradiation time for three energies of incident electrons: 27 eV (blue curve), 65 eV (green curve) and 163 eV (red curve). These energies are chosen to lie above the exciton and hole formation energy, determined by the bandgap width of the material (9.4 eV in the case of LiCl [29]). The behavior of the LiCl-related intensity is similar in all cases, showing an exponential decay that reaches its minimum after long irradiation times (900 s in the present case). The reproducibility of the electron-stimulated desorption kinetics is confirmed by performing several electron-stimulated desorption experiments in the same sample. This is achieved by simply moving to a fresh region (Zone 1, 2, 3) of the surface, since the electron beam diameter is around 10 μm and the sample diameter is 1 cm.

The evolution of the LiCl diffraction intensities can be fitted with a bi-exponential decay function (Eq. (1)),

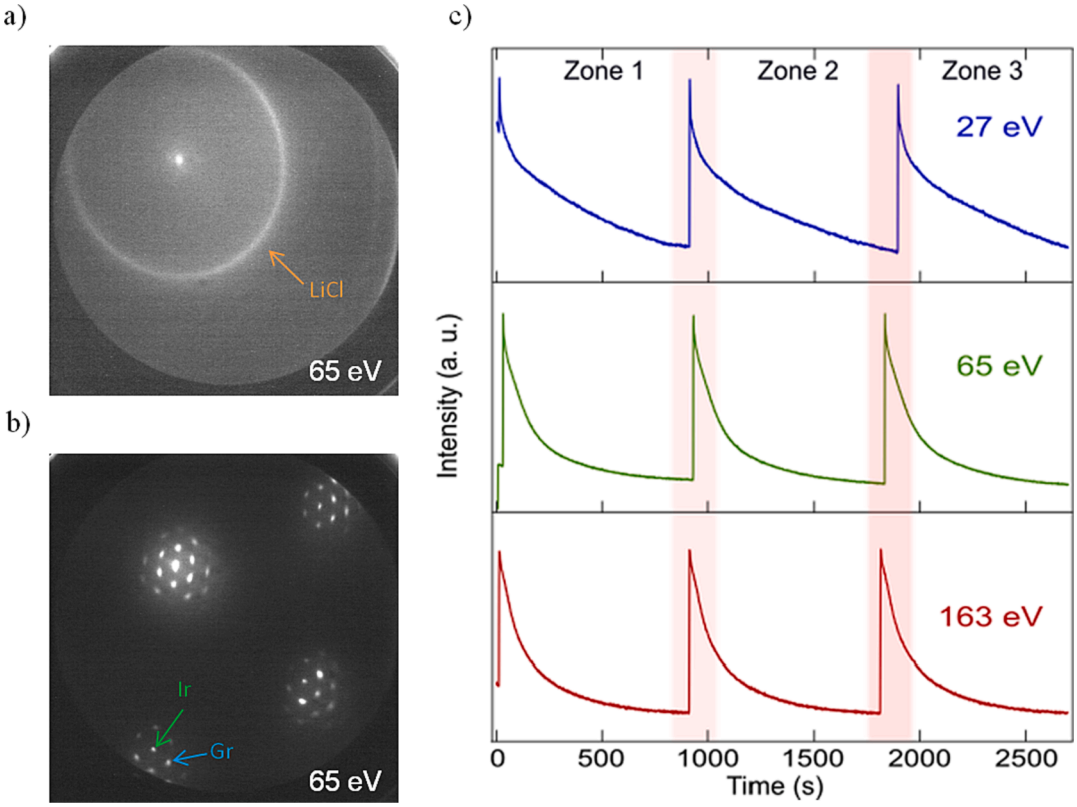

Fig. 1. LEED patterns (E = 65 eV) corresponding to a) initial stage LiCl/Gr/Ir(1 1 1) sample and b) final stage, Gr/Ir(1 1 1) sample. c) Intensity curves of the LiCl ring feature shown by the LEED pattern as a function of irradiation time for electron energies of 27 eV, 65 eV and 163 eV. Three consecutive experiments irradiating three pristine areas are presented for each energy and are marked as zone 1, 2 and 3.

$$I = I_1 e^{-\lambda_1 t} + I_2 e^{-\lambda_2 t} \quad (1)$$

where λ_1 and λ_2 represent the rate coefficients, i. e., the probability of desorption per unit of time and I_1 and I_2 are the normalized desorption intensities (i. e., $I_1 + I_2 = 1$) that correspond to each exponential of the function. As the evolution of the intensity cannot be properly fitted with a single exponential function, two independent desorption mechanisms must be taken into consideration. A fast desorption regime ($I_1 e^{-\lambda_1 t}$) dominates at the beginning of the irradiation (up to 100 s), and a slow desorption regime ($I_2 e^{-\lambda_2 t}$) rules over longer exposure times (beyond 100 s).

Fig. 2 a), b) and c) shows the normalized experimental data (cyan circles) and the fit for the three energies of the incident electrons: 27 eV, 65 eV and 163 eV. We also plot the decomposition of the fit into the two exponential curves (see Figure S1 for a logarithmic representation of the desorption kinetics). The purple curve represents the fast desorption component of the fit and the yellow curve the slow desorption one. The time constants (τ_1 and τ_2) and hence the rate coefficients (λ_1 and λ_2) (Table 1) are in good agreement with those reported in the literature for similar experiments [30]. Fig. 2 d) shows the ratios (λ_1/λ_2) of the rate coefficients. These ratios (λ_1/λ_2) show how efficient is the desorption process of the fast regime in comparison with the one of the slow regime for each energy. In the case of 27 eV, the fast regime is more than 20 times efficient than the slow regime. In the case of 65 eV it is more than 5 times efficient, and in the case of 163 eV it is around 4 times. In conclusion, the lower the energy of the impinging electrons, the more efficient the fast regime process with respect to the slow one is. Analyzing the ratios of the intensities of desorption for each energy (I_1/I_2, see Fig. 2 e) and Table 1), it is noticeable the change in the contribution of each regime: while for the lowest electron energy the intensity of the slow regime is the dominant one, for higher energies is the intensity related to the fast regime the one governing the desorption. This indicates that for low energy electrons (27 eV) most of the material is desorbed slowly, while for higher energy electrons (65 eV and 163 eV) most of the material is desorbed rapidly. It is important to note that Fig. 2 e) shows the intensity ratios, i. e., the relation between the fast and the slow regime in terms of the weight of each regime in the whole desorption process. In the case of 27 eV, 30% of the total desorption takes place within the fast regime whereas this behavior changes for higher energies: 68%, and the 56% for 65 eV and 163 eV respectively; the red line in Fig. 2 e) marks this change.

LiCl desorption can also be traced by imaging the sample with backscattered electrons and studying the transition from mirror electron microscopy (MEM) to LEEM mode. In MEM mode, low-energy electrons are reflected before interacting with the sample surface, and are deflected by the field variations. With increasing energy, electrons interact with the surface (scatter and diffract), entering the LEEM mode. Fig. 3 a) presents an image acquired in MEM mode (relative electron energy = -2 eV) at an irradiated area (brown circle) where LiCl has been mostly desorbed and lithium clusters are present,(alkali cluster formation in addition to desorption upon electron irradiation has already been reported [30]) as evidenced by the increase of the background signal observed in the LEED pattern (see Figure S2). The same zone measured in LEEM mode (relative electron energy = 0 eV) is shown in Fig. 3 b). While in MEM mode the LiCl-desorbed area is almost imperceptible, in LEEM mode the electron-induced damage is clearly visible. The contrast between LiCl-desorbed and pristine LiCl zones is originated from the difference in work functions (Φ).

The contrast mechanisms are schematically depicted in Fig. 3 c), where the left part (brown) represents the irradiated area (LiCl-desorbed area with scarce disordered Li clusters) and the right part the LiCl-covered regions (e. g. area in the blue circle). Due to the lower Φ of the irradiated zone, electrons with lower energy can interact with the surface. While the irradiated zone is in LEEM mode, the LiCl-covered zone is still in MEM mode, where there is total reflection and thus higher intensity. The difference of the MEM-LEEM transition energy between the areas is shown in Fig. 3 d). The intensity of the reflected electrons is plotted as a function of the relative electron energy. The

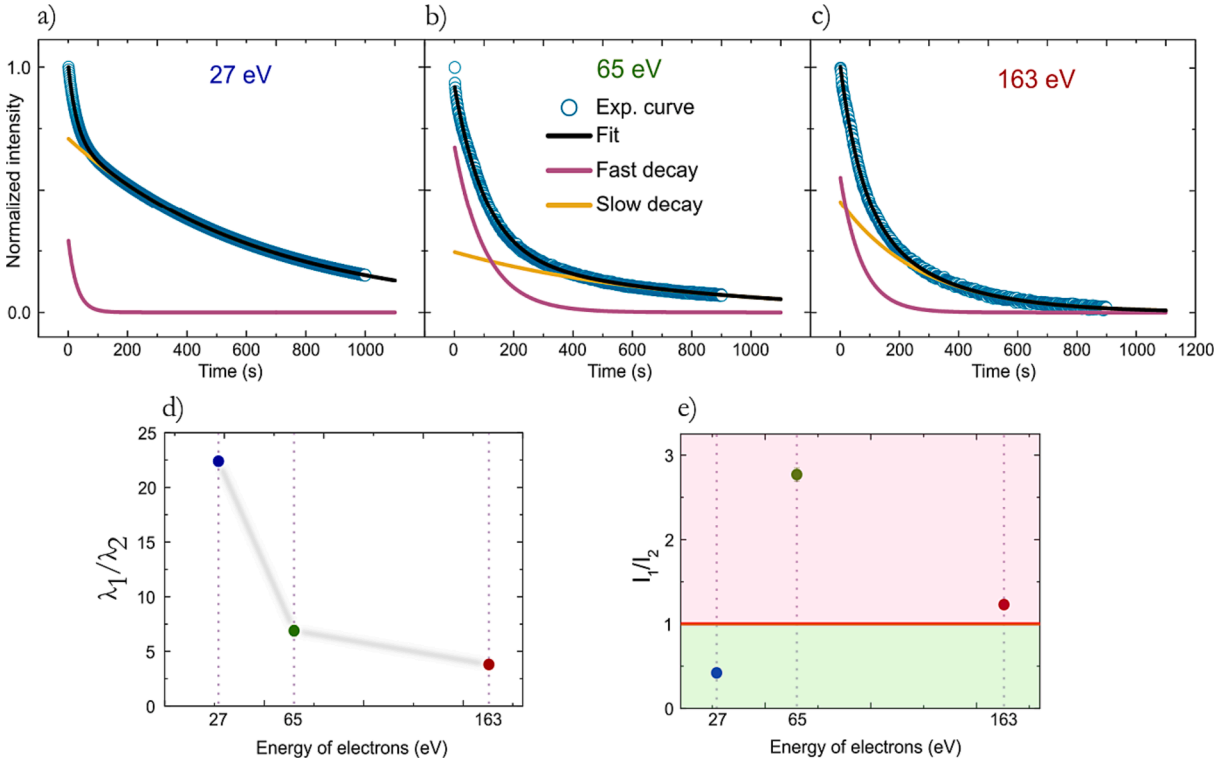

Fig. 2. Fit of the normalized LiCl-related LEED intensity decay for electrons of energy a) 27 eV, b) 65 eV and c) 163 eV. The fit is decomposed in two exponential curves with different time-constants being λ_1 fast and λ_2 slow, respectively. Ratios of the d) rate coefficients (λ_1/λ_2) and of the e) normalized intensities (I_1/I_2) for the three electron energies under study. The red line marks a change in the desorption behavior.

Table 1
Fitting parameters of the bi-exponential decay functions of the intensity decay curves and the ratios of the intensities and desorption rates for incident electrons of 27, 65, 163 eV.

Energy (eV)	I_1	I_2	τ_1 (s)	τ_2 (s)	λ_1 (1/s)	λ_2 (1/s)	I_1/I_2	λ_1/λ_2
27	0.301 ± 0.001	0.710 ± 0.001	28.8 ± 0.1	646 ± 1	0.0347 ± 1.10^{-4}	0.001548 ± 3.10^{-6}	0.42 ± 0.02	22.4 ± 0.1
65	0.681 ± 0.009	0.246 ± 0.004	105 ± 1	725 ± 89	0.0095 ± 1.10^{-4}	0.0014 ± 1.10^{-4}	2.77 ± 0.08	6.8 ± 0.7
163	0.560 ± 0.009	0.454 ± 0.009	72 ± 1	274 ± 6	0.0138 ± 2.10^{-4}	0.00365 ± 1.10^{-5}	1.23 ± 0.04	3.8 ± 0.1

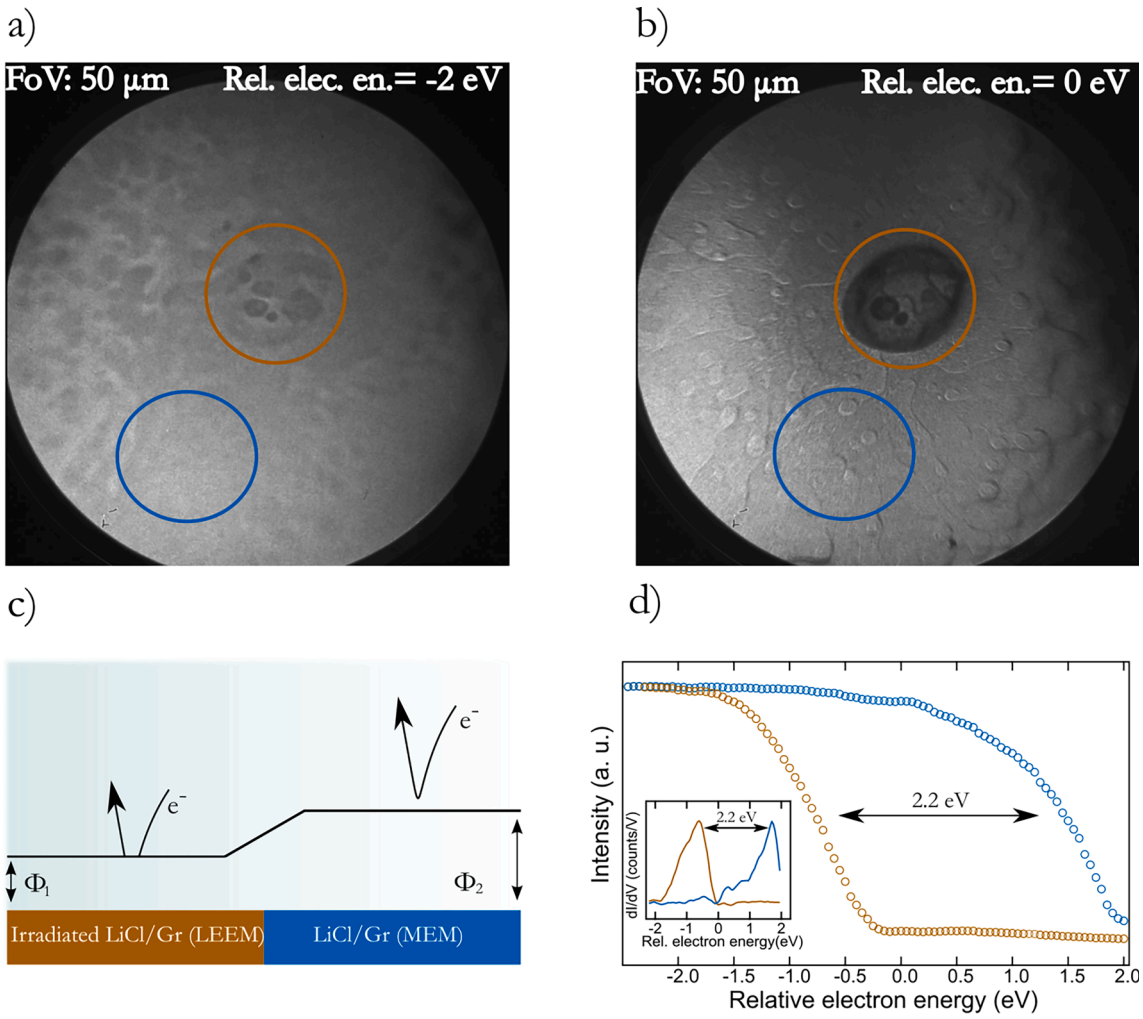

Fig. 3. a) Mirror Electron Microscopy (MEM) image measured biasing the sample and thus tuning the relative electron energy to −2 eV, FoV (i. e., diameter of the circle of the inspected area) = 50 µm b) LEEM image with relative electron energy of 0 eV, FoV = 50 µm. In both images, brown circle points the irradiated zone and blue circle points the non-irradiated zone. c) Representation of the contrast in the image due to differences in the local Work Function (Φ) of the surface. d) Curves extracted from the MEM-LEEM transition image sequence: blue curve was obtained from the area pointed by the blue circle in a) and b) and brown circle was obtained from the area pointed by the brown circle. Inset: derivative of the curves. The maxima of the curves represent the relative electron energy where electrons arrive to the sample with E = 0 eV.

brown curve has been obtained from the irradiated area and the blue curve has been acquired from the LiCl-covered area (LiCl surface). The intensity drop (indicative of the MEM-LEEM transition) of the irradiated surface takes place at a lower energy than that of the LiCl-covered one. The MEM-LEEM transition can be easily quantified from the position of the maximum peaks of the derivatives (inset in Fig. 3 d)) and the difference in Φ between the irradiated and the LiCl-covered zones can be determined. We find a difference in Φ of 2.2 eV between the LiCl film and the irradiated area in agreement with other similar systems reported in the literature [31–33].

After examining the modification of the work function of ultra-thin LiCl films, we turn to the origin of the two mechanisms involved in the desorption process. We compare the evolution when irradiated with soft X-ray photons ($h\nu = 136$ eV). When samples are illuminated with X-rays, we also observe efficient desorption of the ultra-thin LiCl film [7–9]. However, in this case, the kinetic is governed by a single exponential decay, suggesting that only one of the two desorption mechanisms present in electron-induced desorption takes place. Fig. 4 a) shows the normalized intensity decay and the fitting curves of photon- and electron-stimulated desorption of an ultra-thin LiCl film. The time constant and rate coefficient obtained for the photon irradiation point to a fast desorption: $\tau_{X\text{-ray}} = 36.9 \pm 0.8$ s and $\lambda_{X\text{-ray}} = 0.0272 \pm 6.10^{-4}$ s^{-1} with similar values to the ones obtained with electron irradiation (see Table 1) for the fast regime. In addition, it has been reported that irradiation with soft X-ray photons of LiCl and NaCl films on graphene results in the dissociation of the alkali halide layer, the desorption of the

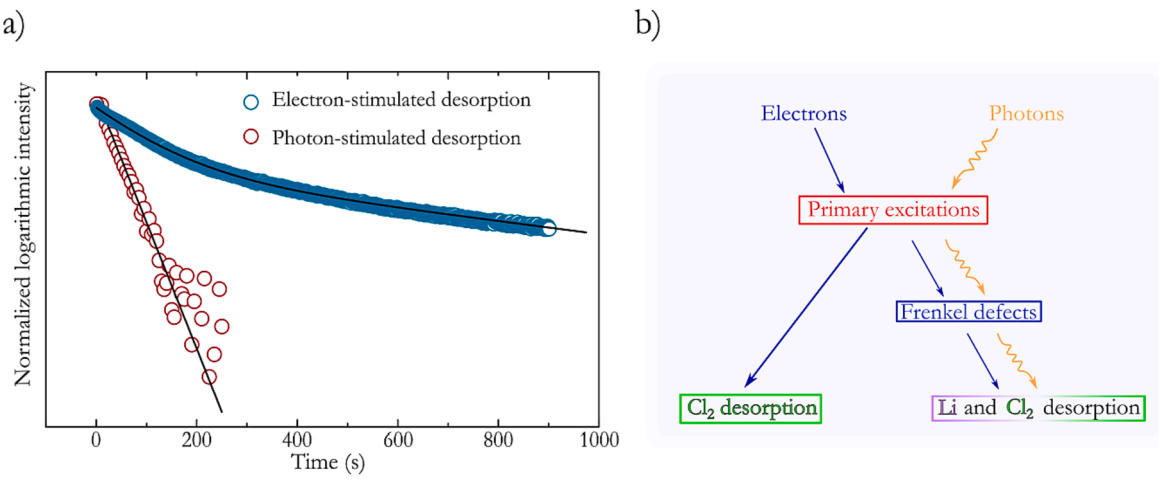

Fig. 4. A) photon- and electron-stimulated LiCl desorption curves and their fits. c) scheme of the electron- and photon-stimulated desorption processes in a lithium chloride thin film.

halogen and the intercalation of a fraction of alkalis into graphene [7,8], decoupling it from the substrate. In our case, this observation is evidenced in LEED by the disappearance of the Gr/Ir(1 1 1) moiré pattern spots once the alkali halide ring is washed away. In the case of electron irradiation, when the LiCl-related LEED ring faints, the moiré pattern-related diffraction spots are recovered, suggesting that lithium intercalation does not take place.

Kolodziej and Szymoski [16] proposed a model composed of two routes for explaining the electron mediated desorption process in a salt crystal. When electrons with a kinetic energy above the bandgap hit the crystal surface, they create primary excitations (holes and excitons). On the one hand, the excess in kinetic energy of these free excitons and hot holes enables the migration of a fraction of the primary excitations to the surface, where direct desorption of principally chlorine occurs. This route, called the nonthermal desorption, is a non-equilibrium process. On the other hand, another fraction of the primary excitations can lead to the production of Frenkel defects, i. e., excited F*-centers, ground state F-centers and H-center pairs [34]. F*-centers and H-centers diffuse to the surface through interactions with phonons. F*-centers neutralize surface alkali ions causing their desorption, while H-centers cause the desorption of surface halogen atoms. This equilibrium process is known as thermal desorption [20] (see Fig. 4 (b) and Figure S3). F-centers in the ground state cannot efficiently diffuse and only secondary absorption of incident electrons or photons may trigger their migration to the surfaces by interaction with phonons [34].

When irradiating with electrons, both thermal and nonthermal mechanisms are present, leading to unbalanced specie desorption, as more chlorine is desorbed. However, when irradiating with photons only the thermal desorption process is activated [16]. Impinging photons, in the same way as electrons, generate hot holes and excitons, but at a much slower rate [9]. Each absorbed photon generates a single free excitation (with a lifetime of 10^{-10} – 10^{-12} s [35]). The probability to produce secondary excitons is remarkably small. In this scenario, the desorption of chlorine and lithium is more balanced.

Taking into account the time constants of the two characteristic regimes (Table 1), the thermal process can be paired with the slow regime whereas the nonthermal can be paired with the fast one. Although the thermal process is slower than the nonthermal one, the photon-stimulated desorption is faster due to the absence of lithium clusters on the surface, which affects to the desorption efficiency [30]. In addition, it has recently been reported that a fraction of alkali atoms intercalate through graphene [8], which favors the constant desorption kinetics.

Since we observe that no lithium intercalation is occurring when irradiating with electrons, we now unveil the origin of this process. In addition to the evolution of primary excitations, the main difference between X-ray and electron-stimulated desorption processes is the following: photons create photoelectrons that deplete from the LiCl film, charging it positively. In contrast, electron irradiation charges the LiCl film negatively. It is important to note that the flux of electrons and photons is very similar ($\approx 10^9$particles/s. μm^2) and thus we discard any key effect coming from this parameter (see Supplementary Information). As the Gr/Ir(1 1 1) substrate is connected to a reference voltage, a potential difference is generated between the LiCl thin film and the Gr/Ir (1 1 1) substrate. In the case of photon irradiation, the electric field attracts Li^+ ions to the interface, where they intercalate through defects and grain boundaries. The direction of the electric field is the opposite for electron irradiation, preventing Li^+ ions from reaching the Gr/Ir (1 1 1) interface and effectively inhibiting Li intercalation under graphene (see Figure S3).

4. Conclusions

In summary, we have analyzed the desorption kinetics of ultra-thin LiCl films on graphene irradiated with low-energy electrons by analyzing the variation of the intensity of its diffraction spots. Electron-induced dissociation kinetics is dominated by a fast and slow desorption regimes with different time scales due to the evolution of the surface of the thin film, where the increase of disordered alkali metal clusters derives in a lower dissociation efficiency. MEM-LEEM imaging shows changes in the work function of the electron-irradiated zone with respect to the pristine LiCl film, confirming the desorption observed by the evolution of the LEED pattern. We have compared the electron-induced desorption kinetics with photon-induced desorption and found that although both irradiation procedures create similar primary excitations, but differences in their final products remaining at the surface are due to the different desorption efficiency of the alkali with respect to the halogen. When irradiating with electrons, there is an increase in the relative concentration of the alkali atoms on the surface. On the contrary, photon irradiation leads to an efficient dissociation of LiCl and a subsequent Li intercalation, increasing the halogen desorption efficiency. Finally, we propose that intercalation of lithium does not occur when irradiating with electrons due to the formation of an electric field in the LiCl film that prevents Li^+ to reach the interface and so inhibits intercalation.

CRediT authorship contribution statement

Jon Azpeitia: Investigation, Formal analysis, Writing – original draft, Writing – review & editing. **Michael Foerster:** Investigation,

Writing – review & editing. **Lucía Aballe:** Investigation, Writing – review & editing. **Mar García-Hernández:** Writing – review & editing. **José Ángel Martín-Gago:** Writing – review & editing. **Pablo Merino:** Investigation, Writing – original draft, Writing – review & editing. **Irene Palacio:** Conceptualization, Investigation, Formal analysis, Writing – original draft, Writing – review & editing.

Declaration of Competing Interest

The authors declare that they have no known competing financial interests or personal relationships that could have appeared to influence the work reported in this paper.

Data availability

Data will be made available on request.

Acknowledgments

This work was supported by the EU Graphene Flagship funding (Grant Graphene Core3 881603). The authors acknowledge financial support from projects RYC2020-029800-I, PID2021-125309OA-I00, PID2020-113142RB-C21, CNS2022-135658 TED2021-129999B-C31 and TED2021-129416A-I00 funded by MCIN/AEI/10.13039/501100011033 and EUR2021-122006.

Appendix A. Supplementary data

Supplementary data to this article can be found online at https://doi.org/10.1016/j.apsusc.2023.158231.

References

[1] K.S. Novoselov, A. Mishchenko, A. Carvalho, A.H. Castro Neto, 2D materials and van der waals heterostructures, Science 353 (2016) aac9439.
[2] J. Repp, G. Meyer, F.E. Olsson, M. Persson, Controlling the charge state of individual gold adatoms, Science 305 (2004) 493–495.
[3] J. Repp, G. Meyer, S.M. Stojković, A. Gourdon, C. Joachim, Molecules on insulating films: Scanning-tunneling microscopy imaging of individual molecular orbitals, Phys. Rev. Lett. 94 (2005) 026803.
[4] K. Schouteden, K. Lauwaet, E. Janssens, G. Barcaro, A. Fortunelli, C. Van Haesendonck, P. Lievens, Probing the atomic structure of metallic nanoclusters with the tip of a scanning tunneling microscope, Nanoscale 6 (2014) 2170.
[5] I. Palacio, K. Lauwaet, L. Vázquez, F.J. Palomares, H. González-Herrero, J. I. Martínez, L. Aballe, M. Foerster, M. Garciá-Hernández, J.Á. Martín-Gago, Ultra-Thin NaCl films as protective layers for graphene, Nanoscale 11 (2019) 16767.
[6] S. Fatayer, B. Schuler, W. Steurer, I. Scivetti, J. Repp, L. Gross, M. Persson, G. Meyer, Reorganization energy upon charging a single molecule on an insulator measured by atomic force microscopy, Nat. Nanotechnol. 13 (2018) 376.
[7] I. Palacio, J.A. Martin-Gago, L. Aballe, M. Foerster, D.G. de Oteyza, M. Garcia-Hernandez, Reversible Graphene Decoupling by NaCl Photo-Dissociation, 2D Mater. 6 (2019), 025021.
[8] J. Azpeitia, P. Merino, S. Ruiz-Gómez, M. Foerster, L. Aballe, M. García-Hernández, J.Á. Martín-Gago, I. Palacio, LiCl photodissociation on graphene: A photochemical approach to lithium intercalation, ACS Appl. Mater. Interfaces 13 (2021) 42205.
[9] M. Szymonski, J. Kolodziej, P. Czuba, P. Korecki, P. Piatkowski, Z. Postawa, M. Piacentini, N. Zema, Photon stimulated desorption from alkali halide surfaces at near threshold energies, Surf. Sci. 363 (1996) 229.
[10] V.N. Ageev, Y.A. Kuznetsov, Electron-stimulated desorption of potassium and cesium atoms from an oxidized molybdenum surface, Phys. Solid State 39 (1997) 671.
[11] T. Yasue, A. Ichimiya, S. Ohtani, Electron stimulated desorption of positive ions from alkali halide surfaces, Surf. Sci. 186 (1987) 191.
[12] V.N. Ageev, Y.A. Kuznetsov, B.V. Yakshinskii, T.E. Madey, Electron stimulated desorption of alkali metal ions and atoms: local surface field relaxation, Nucl. Inst. Methods Phys. Res. B 101 (1995) 69.
[13] V.N. Ageev, Y.A. Kuznetsov, Electron-stimulated desorption of sodium atoms from oxidized molybdenum surface, Phys. Rev. B 58 (1998) 2248.
[14] P. Wurz, J. Sarnthein, W. Husinsky, G. Betz, P. Nordlander, Y. Wang, Electron-stimulated desorption of neutral lithium atoms from LiF due to excitation of surface excitons, Phys. Rev. B 43 (1991) 6729.
[15] P.R. Antoniewicz, Model for electron- and photon-stimulated desorption, Phys. Rev. B 21 (1980) 3811.
[16] J. Kolodziej, M. Szymonski, Hot-carrier transport processes in stimulated desorption of alkali halides, Phys. Rev. B - Condens. Matter Mater. Phys. 58 (1998) 13204.
[17] M. Szymonski, J. Kolodziej, B. Such, P. Piatkowski, P. Struski, P. Czuba, F. Krok, Nano-scale modification of ionic surfaces induced by electronic transitions, Prog. Surf. Sci. 67 (2001) 123.
[18] Y. Shapira, Dynamics of surface atoms and molecules under irradiation, Isr. J. Chem. 22 (1982) 386.
[19] R.T. Williams, Creation of lattice defects in the bulk and at the surface of alkali halide crystals, Radiat Eff. Defects Solids 109 (1989) 175.
[20] M. Szymonski, J. Kolodziej, P. Czuba, P. Piatkowski, A. Poradzisz, N.H. Tolk, J. Fine, New mechanism for electron-stimulated desorption of nonthermal halogen atoms from alkali-halide surfaces, Phys. Rev. Lett. 67 (1991) 1906.
[21] S. Ichinokura, A. Hemmi, H. Cun, K. Tanaka, R. Shimizu, T. Hitosugi, T. Greber, T. Hirahara, Efficiency of electron doping to monolayer hexagonal boron nitride by alkali metals, Appl. Phys. Lett. 122 (2023), 071601.
[22] Z. Wang, R. Li, C. Su, K.P. Loh, Intercalated phases of transition metal dichalcogenides, SmartMat 1 (2020) e1013. https://onlinelibrary.wiley.com/doi/full/10.1002/smm2.1013.
[23] F. Gołek, W.J. Sobolewski, Thresholds of ESD for LiF thin layers, Vacuum 63 (2001) 3.
[24] F. Golek, ESD thresholds for KCl, Phys. Status Solidi Basic Res. 239 (2003) 336.
[25] F. Gołek, ESD thresholds for NaCl, Appl. Surf. Sci. 225 (2004) 267.
[26] L. Aballe, M. Foerster, E. Pellegrin, J. Nicolas, S. Ferrer, The ALBA spectroscopic LEEM-PEEM experimental station: Layout and performance, J. Synchrotron Radiat. 22 (2015) 745.
[27] J. Coraux, A.T. N'Diaye, M. Engler, C. Busse, D. Wall, N. Buckanie, F.J. Meyer Zu Heringdorf, R. Van Gastel, B. Poelsema, T. Michely, Growth of Graphene on Ir (111), New J. Phys. 11 (2009), 023006.
[28] H. Hattab, A.T. N'Diaye, D. Wall, G. Jnawali, J. Coraux, C. Busse, R. Van Gastel, B. Poelsema, T. Michely, F.J. Meyer Zu Heringdorf, M. Horn-Von Hoegen, Growth temperature dependent graphene alignment on Ir(111), Appl. Phys. Lett. 98 (2011) 141903.
[29] A.B. Kunz, Study of the electronic structure of twelve alkali halide crystals, Phys. Rev. B 26 (1982) 2056.
[30] A. Husseen, S. Le Moal, H. Oughaddou, G. Dujardin, A. Mayne, E. Le Moal, Reaction kinetics of ultrathin NaCl films on Ag(001) upon electron irradiation, Phys. Rev. B 96 (2017) 235418.
[31] B. Naydenov, L. Surnev, Sodium adsorption on a Ge(100)-(2 × 1) surface, Surf. Sci. 370 (1997) 155.
[32] M. Tikhov, G. Boishin, L. Surnev, Sodium adsorption on a Si(100)-(2 × 1) surface, Surf. Sci. 241 (1991) 103.
[33] K. Akada, S. Obata, K. Saiki, Work function lowering of graphite by sequential surface modifications: Nitrogen and hydrogen plasma treatment, ACS Omega 4 (2019) 16531.
[34] M. Szymonski, A. Droba, P. Struski, F. Krok, Dynamics of the defect-mediated desorption of alkali halide surfaces, Low Temp. Phys. 38 (2012) 774.
[35] M.A. Elango, V.N. Kadchenko, A.M.E. Saar, A.P. Zhurakovski, Thermoluminescence light sum storage in NaCl : Ag by ultrasoft X-rays, J. Lumin. 14 (1976) 375.